Korean J. Chem. Eng., 33(2), 720-725 (2016)
DOI: 10.1007/s11814-015-0181-0

pISSN: 0256-1115
eISSN: 1975-7220

Enhanced adsorption of fluoride from aqueous solutions by hierarchically structured Mg-Al LDHs/Al_2O_3 composites

Tao Zhang*,, Hanqiang Yu**, Yuming Zhou*,†, Jian Rong**, Zhanyu Mei*, and Fengxian Qiu**,†**

*School of Chemistry and Chemical Engineering, Southeast University,
Jiangsu Optoelectronic Functional Materials and Engineering Laboratory, Nanjing 211189, China
**School of Chemistry and Chemical Engineering, Jiangsu University, Zhenjiang 212013, China
(*Received 26 May 2015 • accepted 21 August 2015*)

Abstract−Hierarchically structured layered double hydroxides (LDHs)/Al_2O_3 composites were fabricated from waste paper fibers using a two-step method. In the first step microscaled Al_2O_3 fibers were prepared by template-directed synthesis employing waste paper fibers as templates; and in the second step nanoscaled LDHs platelets were fabricated into hierarchical architectures based on crystal growth on Al_2O_3 fibers surface. The morphology and structure of as-prepared samples were characterized by scanning electron microscopy (SEM), N_2 adsorption/desorption analysis and X-ray diffraction (XRD) analysis. The SEM results revealed that the inorganic fibers were covered by LDHs platelets, forming the hierarchical structures with micro- to nanoscales. The BET analysis showed that the surface area was increased from 76.66 m^2/g (Al_2O_3 fibers) to 165.0 m^2/g (composites) by the growth of LDHs platelets on the surfaces of Al_2O_3 fibers. As compared to bare LDHs particles and Al_2O_3 fibers, the LDHs/Al_2O_3 composites show a high fluoride adsorption capacity, and the maximum adsorption capacity can reach up to 58.7 mg/g. The Langmuir isotherm model was found to agree well with the equilibrium data, while the pseudo-second order model provided the highest correlation of the kinetic data for fluoride adsorption. The as-prepared LDHs/Al_2O_3 composites and corresponding design strategies developed herein are expected to be applicable to the synthesis of other LDHs based composites for the removal of pollutants from water.

Keywords: Mg-Al LDHs/Al_2O_3, Hierarchical Structures, Waste Paper, Adsorption, Fluoride

INTRODUCTION

Increasing public concern regarding energy consumption and environmental pollution has led to the development of renewable and eco-friendly materials. Much attention has been focused on the development of paper-based materials because its source (cellulose) is abundant in nature, low cost, and environmentally benign [1]. However, the increasing use of paper-based materials has produced large amounts of waste paper. The utilization of waste paper for pollution control has recently been reported as a potential alternative to the synthetic materials. In this regard, several adsorbents like waste paper pulp [2], chemically modified waste paper [3], paper industry waste material [4] have been studied for the removal of heavy metals ions from aqueous solutions. In addition, Okada et al. [5] used the waste paper to prepare activated carbons by chemical and physical activation. However, the use of waste paper for fabricating hierarchically porous composite adsorbent has not been previously reported.

Fluoride contamination in drinking water has become a serious environmental problem due to natural and anthropogenic activities [6], which have posed significant risks to human and animal health. Long-term ingestion of high fluoride drinking water may lead to dental fluorosis, skeletal fluorosis and even crippling skeletal fluorosis [7]. According to the World Health Organization (WHO) guidelines [8], the fluoride concentration recommended for potable water for human consumption is generally in the range of 0.5 mg/L to 1.5 mg/L. However, high-fluoride levels in groundwater are found in many parts of world, particularly in China, India, Africa and Mexico [9]. Therefore, the efficient treatment of excess amount of fluoride from drinking water is extremely important to protect public health. Numerous methods have been developed for remove excessive fluoride from drinking water such as ion exchange [10], adsorption [7], nanofiltration [11], and electrodialysis [12]. Among these, adsorption is highly effective due to being economical, simple and energy saving.

Many adsorbents such as rare earth oxides [6], LDHs [13] and activated alumina [14] have been used to remove excessive fluoride from water. Rare earth-based adsorbents have been confirmed to have high sorption capacity for fluoride [15]. Rare earth metals have been used to modify conventional adsorbents to prepare the composite adsorbents [16]. However, the prices of these adsorbents should be considered in practical application. The heavy metal pollution derived from rare earth elements should also be considered in adsorbent preparation and adsorption process. Though fluoride adsorption on LDHs and Al_2O_3 is evident by some research workers, there are no reports on the preparation of hierarchically structured LDHs/Al_2O_3 composites for fluoride removal from aqueous solutions. Enhanced fluoride adsorption properties could possibly

†To whom correspondence should be addressed.
E-mail: fchem@163.com, fxqiu@126.com

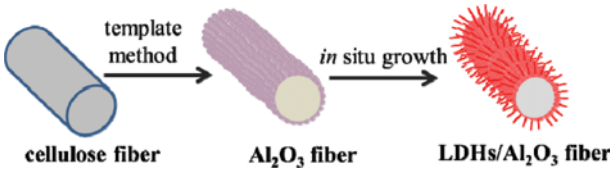

Scheme 1. Schematic illustration of the preparation of LDHs/Al_2O_3 fiber using waste paper fibers as templates.

be achieved by the combination of the hierarchical structures of composites with the functionality of LDHs and Al_2O_3. We fabricated hierarchically porous LDHs/Al_2O_3 composites from waste paper fibers using a two-step method. In the first step the microscaled Al_2O_3 fibers are prepared by template-directed synthesis employing paper fibers as templates, and in the second step the nanoscaled LDHs platelets are fabricated into hierarchical architectures by in situ growth on Al_2O_3 fibers surface. The synthesis process of hierarchical LDHs/Al_2O_3 fiber composites is illustrated in Scheme 1. The fabricated composites exhibit special surface structures, offering the combined benefit of the unique electrostatic interaction and high surface areas, which have promising application in water treatment.

EXPERIMENTAL SECTION

1. Preparation of Hierarchically Porous Mg-Al LDHs/Al_2O_3 Composites

Waste papers were recycled from daily life. After being washed several times with distilled water, they were cleaned with absolute ethanol followed by drying at 80 °C for 12 h in a ventilation drying oven. Other reagents (analytical grade) were used as received from commercial suppliers without any further purification. The alumina sol was prepared as described in our previous work [17]. Then, 0.4 g of washed papers was immersed into 200 mL of precursor sol and treated under ultrasound irradiation for 2 h. The infiltrated papers were washed with distilled water to remove non-adsorbed metal ions. After being dried at 80 °C for 12 h, the sample was calcined at 550 °C for 4 h to obtain cellulose fiber-based Al_2O_3 fibers.

The hierarchically porous Mg-Al LDHs/Al_2O_3 composites were fabricated by combining the template method and hydrothermal method. Briefly, 0.512 g of $Mg(NO_3)_2{\cdot}6H_2O$ and 0.560 g of HMT were dissolved in 25 mL of distilled water in a 30 mL autoclave Teflon vessel. Then, 0.102 g of as-prepared Al_2O_3 fiber was immersed in the above mixed solution. The vessel was further treated under a hydrothermal condition at 105 °C for 12 h and subsequently left to cool to room temperature. After the hydrothermal reaction, the obtained sample was filtered, washed with distilled water and ethanol for several times and dried at 120 °C to get the hierarchically porous Mg-Al LDHs/Al_2O_3 composites.

2. Sample Characterization

The morphologies and microstructures of LDHs/Al_2O_3 composites were characterized by obtaining scanning electron microscope images using a Hitachi S-3400N SEM at an acceleration voltage of 20 kV. The general structure of the samples was investigated using an X-ray diffraction measurement on a Bruker-AXS D8 X-ray diffractometer system with Cu Kα radiation at 40 kV and 40 mA. The surface areas and pore-size distributions of prepared products were analyzed by nitrogen adsorption measurements, operated at 77 K on a Micromeritics ASAP 2020 adsorption analyzer. The Brunauer, Emmett, and Teller (BET) equation was used to obtain the specific surface areas.

3. Adsorption Experiments

We measured the concentration of fluoride solution by a fluoride ion-selective electrode (PF-1). Batch process was employed for adsorption studies. The equilibrium adsorption isotherms were as follows: 50 mg of the Mg-Al LDHs/Al_2O_3 composites was added into 50 mL fluoride solution at different initial concentrations.

The amount of fluoride adsorbed at equilibrium, q_e was calculated by Eq. (1).

$$q_e = \frac{(C_0 - C_e)V}{m} \quad (1)$$

where q_e is the adsorption capacity (mg/g) at equilibrium, C_0 and C_e are the initial concentration and equilibrium concentration, respectively. V is the volume (L) of solution and m is the mass (g) of adsorbent used.

RESULTS AND DISCUSSION

Fig. 1(a)-(c) shows the SEM images of the cellulose fiber-based Al_2O_3 prepared by template method. From Fig. 1(a), the Al_2O_3 fibers are interlaced with each other forming the meshwork. The length of the inorganic fibers ranges from tens to several hundred micrometers and the diameter varies from several to tens micrometers. The lengths and dimensions of the Al_2O_3 fibers are not uniform, which may be ascribed to the complexity of waste paper fibers. The magnified SEM images of a single fiber are shown in Fig. 2(b), which proves that the structure of paper fibers has been successfully replicated by template method. Obviously, the microscaled Al_2O_3 fibers can provide enough space for in situ growth nanoscaled LDHs. Fig. 1(c) illustrates the magnified images of Al_2O_3 fiber surfaces, indicating that the fine structures of cellulose fibers are reserved in inorganic replicas.

Fig. 1(d)-(f) shows the morphologies and microstructures of the fabricated Mg-Al LDHs/Al_2O_3 composites. It can be seen from Fig. 1(d) that the unique fibrous structures of the target product are faithfully inherited from that of the Al_2O_3 fibers. The magnified SEM images (Fig. 1(e)) of a single fiber clearly show the diameters of the fiber composites ranges from 5 to 10 μm, approaching that of Al_2O_3 fibers. Compared with the SEM images of the cellulose fiber-based Al_2O_3 fibers displayed in Fig. 1(b), the surface morphology of the inorganic fibers is complicated by the growth of LDH nanosheets. The Al_2O_3 fibers are covered by thousands of flat platelets, indicating the prepared composites show a hierarchical structure at scales ranging from micro- to nanoscales. Fig. 1(f) presents the magnified image of the LDHs nanoplatelets. The results clearly show that the LDHs sheets are dispersed disorderly on the surface of inorganic fibers. Compared with the relatively smooth surfaces of Al_2O_3 fibers (Fig. 1(c)), the LDHs/Al_2O_3 composites contain a large numbers of macroporous on the surfaces of fibers, forming hierarchical structures with high surface-to-volume ratios.

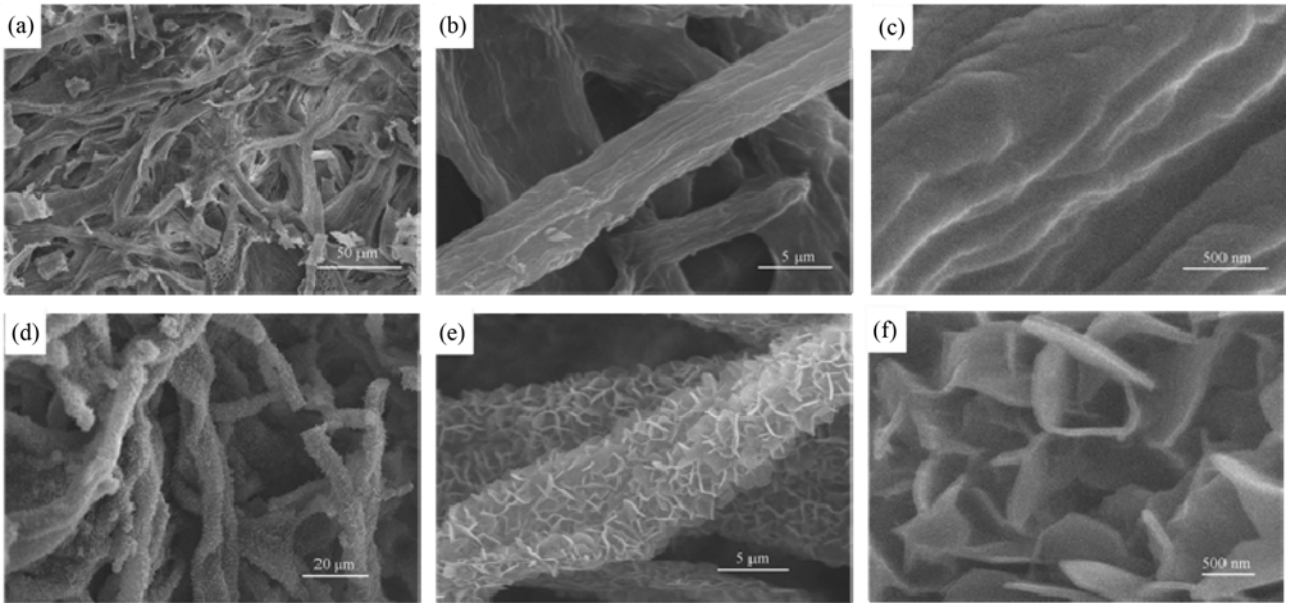

Fig. 1. SEM images of as-obtained (a)-(c) cellulose fiber-based Al_2O_3 fibers and (d)-(f) Mg-Al LDHs/Al_2O_3 composites.

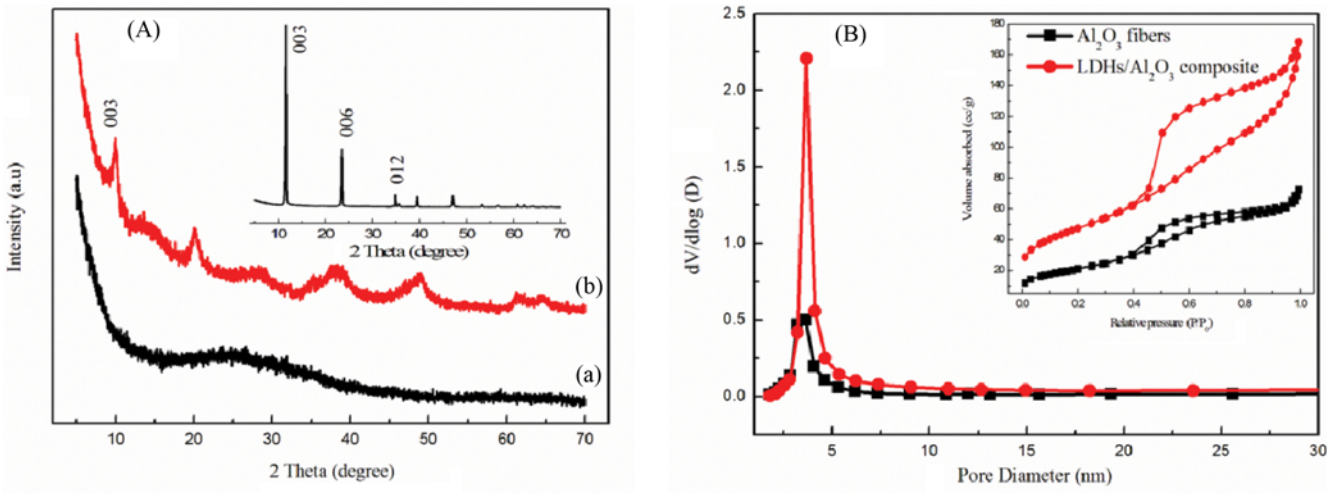

Fig. 2. (A) XRD patterns of as-synthesized (a) Al_2O_3 fibers, (b) Mg-Al LDHs/Al_2O_3 composites and (inset) bare LDHs; (B) BJH pore size distributions and N_2 adsorption-desorption isotherms (inset) of Al_2O_3 fibers and LDHs/Al_2O_3 composites.

The XRD patterns of as-synthesized Al_2O_3 fibers and Mg-Al LDHs/Al_2O_3 composites are shown in Fig. 2(A). The sample of Al_2O_3 fiber shows only very broad and diffuse patterns, which reveals its amorphous nature. To compare the structural changes, the bare Mg-Al LDHs particles are synthesized by hydrothermal method as described previously [18], and the corresponding XRD pattern is shown in inset of Fig. 2(A). The reflections of synthesized LDHs particles show sharp and symmetric peaks, even at a high angle range, indicating the highly crystalline nature of the samples. However, LDHs phase in Mg-Al LDHs/Al_2O_3 composites shows the relatively broad and asymmetric reflections, implying the random and disordered structures of Mg-Al LDHs on the surface of Al_2O_3.

The adsorption capacity of an adsorbent often follows the pore structure and total surface area, since there are usually more available active binding sites on a material with higher surface area. The surface and porosity of the samples were characterized by N_2 adsorption - desorption analysis. Fig. 2(B) shows the pore size distribution and nitrogen adsorption - desorption isotherms of cellulose fiber-based Al_2O_3 fibers and Mg-Al LDHs/Al_2O_3 composites. The BET specific surface areas of cellulose fiber-based Al_2O_3 fibers and composites were measured to be 76.66 m^2/g and 165.0 m^2/g, respectively. The larger surface areas provide more active sites for fluoride adsorption, making the adsorption process more efficient. The significant changes in BET surface areas observed for materials prepared by in situ growth method are attributed to the vertical growth of the LDHs nanosheets on the surface of Al_2O_3. The corresponding pore size distributions indicate that the pore structures are basically mesoporous with pore sizes predominantly less than 30 nm with average pore diameters of ~3.63 nm (Al_2O_3 fibers) and ~3.67 nm (LDHs/Al_2O_3 composites), respectively. The closed

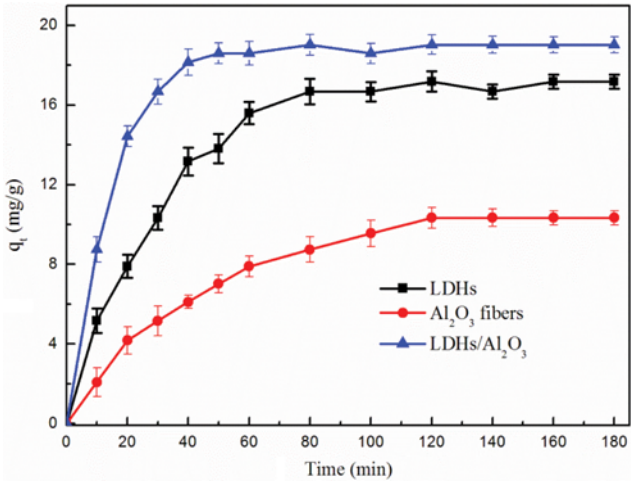

Fig. 3. Comparison of adsorption capacity of fluoride on different adsorbents (conditions: fluoride concentration, 30 mg/L; pH, 5-7; does, 1 g/L and adsorption temperature: 30 °C).

pore diameter may be attributed to the composition of mesoporous Al_2O_3. The isotherms (inset of Fig. 2(B)) present characteristic features of a type IV with a broad H_3 hysteresis loops, indicating the presence of mesopores as well as macropores in morphology analysis. The amount of N_2 adsorbed at the surface of LDHs/Al_2O_3 composites was greater than that of Al_2O_3 fibers, indicating the excellent adsorption properties of composites. Besides, the macroporous structure, ranging from nanometer to micrometer scales, can be directly observed in morphology analysis as shown in Fig. 1(f), which cannot be accessed by N_2 adsorption-desorption analysis.

The positively charged hydroxide sheets are orderly stacked based on the strong electrostatic interaction and hydrogen bonding, resulting in the highly ordered structures and extremely limited interlayer space of LDHs. It is unfavorable for adsorption due to the limited diffusion of adsorbate in the interlayer of the LDHs. The in situ growth technique suggests that the LDHs nanosheets are perpendicular to the substrate materials, which avoid the formation of multilayer stack of LDHs sheets. Fig. 3. shows the comparison of adsorption capacity of fluoride on different adsorbents, confirming the excellent fluoride adsorption properties of the hierarchically structured LDHs/Al_2O_3 composites. The fluoride adsorption capacity could reach up to 19.03 mg/g with the adsorption time of 24 h, accompanied by the initial concentration of fluoride reduces from 30 mg/L to 10.97 mg/L. The adsorption capacity of LDHs/Al_2O_3 composites is two times higher than that of Al_2O_3 fibers under the same adsorption conditions. The fluoride adsorption on LDHs was rapid in the first 60 min and became almost asymptotic after 80 min. However, it took 120 min for Al_2O_3 fibers to reach the adsorption equilibrium. The slower adsorption process for Al_2O_3 may be attributed to a very slow diffusion of the adsorbents from the surface film to micro-pores. The results also revealed that the adsorption of fluoride on the LDHs/Al_2O_3 composites was fast, and the adsorption equilibrium could be attained within 40 min. The fast fluoride adsorption may be attributed to higher surface area and porosity of composites. The fluoride ions are readily diffused into the composites and are rapidly adsorbed on positively charged LDHs

Table 1. Comparison of several reported adsorbents for fluoride removal

Adsorbents	q_{max} (mg g^{-1})	References
Activated alumina	5.4	[6]
Polyaniline/Alumina	5.6	[19]
Kaolin clay	17.8	[20]
Activated red mud	5.7	[21]
La^{3+}-exchanged zeolite F-9	11.0	[22]
Precipitated waste mud	27.2	[23]
Zn–Al layered double hydroxides	1.1–4.2	[5]
Calcined Mg–Al layered double hydroxides	80.1	[24]
Mg-Al LDHs/Al_2O_3 composites	58.7*	This work

*Adsorption conditions: fluoride concentration, 105 mg/L; does, 1 g/L; adsorption time, 24 h and adsorption temperature: 60 °C)

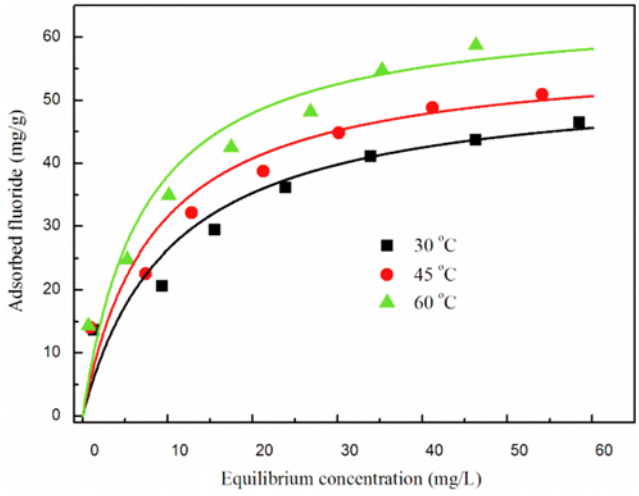

Fig. 4. Experimental equilibrium data (dots) and Langmuir fits (curves) for the fluoride adsorption onto cellulose fiber-based Mg-Al LDHs/Al_2O_3 composites at different temperatures (conditions: fluoride concentration, 15-105 mg/L; pH, 5-7; does, 1 g/L and adsorption time: 24 h).

platelet. Compared with several reported adsorbents (Table 1) for fluoride removal from aqueous solutions, the LDHs/Al_2O_3 composites show a high fluoride adsorption capacity, and the maximum adsorption capacity can reach up to 58.7 mg/g (See Fig. 4).

Equilibrium isotherms are fundamental to understanding the mechanism of fluoride adsorption [25]. The equilibrium distribution of fluoride between the liquid phase and the solid phase is important in determining the fluoride adsorption capacity. To establish the most appropriate correlation for the equilibrium curves, three well-known isotherm models, namely Langmuir, Freudlich and Dubinin-Radushkevich (D-R) equations [15,17,26], were adopted to examine the mechanism of the fluoride adsorption.

The linear form of Langmuir isotherm is expressed as follows:

$$\frac{C_e}{q_e} = \frac{1}{K_L q_m} + \frac{C_e}{q_m} \quad (2)$$

Table 2. Langmuir isotherm model constants and correlation coefficients for adsorption of fluoride onto adsorbents at different temperature

Temperature (°C)	K_L (L/mg)	R^2	q_{max} (mg/g)	q_m (mg/g)
30	0.0971	0.97	46.49	53.39
45	0.1207	0.98	50.88	57.60
60	0.1400	0.98	58.68	65.02

The Freundlich isotherm is an empirical equation based upon the assumption of multilayer formation of adsorbate onto a heterogeneous surface adsorbent [3]:

$$\ln q_e = \ln K_F + \frac{1}{n}\ln C_e \quad (3)$$

The D-R isotherm is more general than the Langmuir isotherm, which was proposed by Dubinin and Radushkevich [27]. From the model, the adsorption on a single type of uniform pores can be applied to distinguish between physical and chemical adsorption [28]:

$$\ln q_e = \ln q_{max} - \beta\varepsilon^2 \quad (4)$$

The effect of adsorption temperatures on fluoride adsorption was studied in the range of 30-60 °C at initial fluoride concentrations ranging from 15 to 105 mg/L. Fig. 4 shows the experimental equilibrium data and Langmuir fits (curves) for the fluoride adsorption onto composites at different temperatures. The calculated values for Langmuir parameters are summarized in Table 2. As shown in Fig. 4, the adsorption capacity was increased with increasing fluoride concentrations and became almost asymptotic at higher concentrations. These curves indicate that the Langmuir isotherm model is consistent with the data at different adsorption temperatures. The fact was further supported by the correlation coefficient (R^2) in Table 2. However, the theoretical maximum adsorption capacity (q_m) was slightly increased as compared to the maximum experimental value (q_{max}), which may be attributed to the increasing trend of fitted curves. Note that adsorption capacity increased with increasing temperature, indicating the endothermic nature of the adsorption process. This is in agreement with the results of Langmuir parameter that the K_L was increased with increasing temperature.

Table 3 presents the values of correlation coefficients and constants of Freundlich and D-R isotherm model for the adsorption of fluoride. The isotherms are not to be linear as evidenced from the values of correlation coefficients. Hence the adsorption equilibrium data do not exactly fit the Freundlich and D-R models.

To determine the adsorption kinetics and rate-limiting step during adsorption process, the effects of adsorption time obtained from different initial fluoride concentration were further analyzed by different kinetic models. These models, including the pseudo-first-order model, pseudo-second-order model, and intraparticle diffusion [29-31], were used to fit the experimental data:

$$\ln(q_e - q_t) = \ln q_e - k_1 t \quad (5)$$

$$\frac{t}{q_t} = \frac{1}{k_2 q_e^2} + \frac{t}{q_e} \quad (6)$$

$$q_t = k_p t^{1/2} + C \quad (7)$$

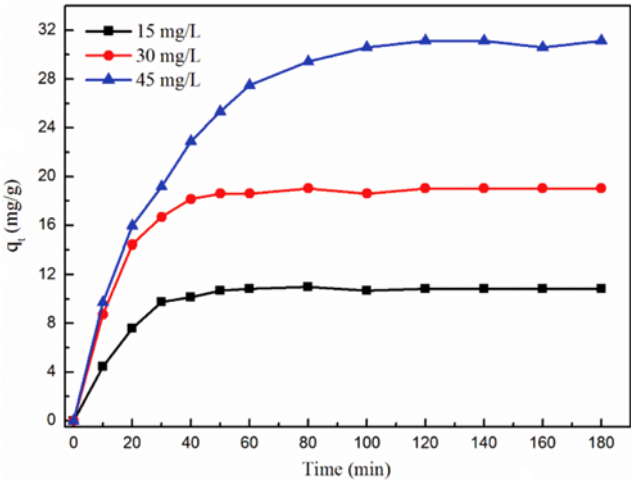

Fig. 5. Adsorption kinetics of fluoride on the Mg-Al LDHs/Al_2O_3 composites at different initial fluoride concentration (conditions: fluoride concentration, 15-45 mg/L; pH, 5-7; does, 1 g/L and adsorption temperature: 30 °C).

Fig. 5 shows the effect of adsorption time on the amount of adsorbed fluoride on composites. The results show that the adsorption equilibrium could be reached within 100 min. Note that the time required for reaching adsorption equilibrium increased from 40 min to 100 min with the fluoride concentration increased from 15 mg/L to 45 mg/L. The slow adsorption at higher fluoride concentrations was further confirmed by the calculated rate constants as shown in Table 4. In the fluoride adsorption process, the adsorption sites of composites were occupied by the adsorbed fluoride ions. It is a slow process to adsorb the excess fluoride ions on nearly saturated adsorption sites. This might explain the decrease in rate constants with increase in fluoride concentration. In addition, from Fig. 5, the fluoride adsorption capacity was increased with increasing fluoride concentration.

Table 3. Freundlich and Dubunin-Radushkevich isotherm model constants and correlation coefficients for adsorption of fluoride onto adsorbents at different temperature

Temperature (°C)	Freundlich			Dubunin-Radushkevich
	R^2	n	K_F (mg/g (L/mg)$^{1/n}$)	R^2
30	0.96	2.906	11.51	0.65
45	0.97	3.003	13.67	0.67
60	0.99	2.898	15.54	0.69

Table 4. Kinetic parameters for adsorption of fluoride onto LDHs/Al_2O_3 composites

Model	Pseudo-first-order			Pseudo-second-order			Intraparticle diffusion	
Parameters	R^2	K_1 (min^{-1})	$q_{e(cal)}$ (mg/g)	R^2	K_2 (g mg^{-1} min^{-1})	$q_{e(cal)}$ (mg/g)	R^2	K_p (mg g^{-1} $min^{-1/2}$)
15 mg/L	0.90	2.35×10^{-2}	9.78	0.98	3.31×10^{-3}	14.98	0.96	1.50
30 mg/L	0.91	3.63×10^{-2}	13.44	0.99	2.94×10^{-3}	23.77	0.95	2.55
45 mg/L	0.97	2.42×10^{-2}	31.64	0.99	6.62×10^{-4}	43.12	0.99	3.63

A comparison of the kinetic data with the linearized plot of those models is presented in Table 4. The results indicate that the pseudo-second-order kinetic model was followed better than pseudo-first-order and intraparticle diffusion kinetic model according to the high correlation coefficient (R^2>0.98). The experimental data fitted well to the second-order kinetic model, which indicates that chemical adsorption is the rate-limiting step, instead of mass transfer.

CONCLUSIONS

Hierarchically porous LDHs/Al_2O_3 composites with porous structures were successfully fabricated by combining the template method and hydrothermal method. This environmentally friendly strategy not only involves the replication the fiber structures to obtain morph-Al_2O_3, but also involves the fabrication of 2D LDHs nanoplatelets into complex 3D architectures. The amorphous Al_2O_3 fibers are obtained by template-directed synthesis employing waste paper fibers as templates. After hydrothermal treatment, the amorphous Al_2O_3 fibers change into crystalline structures composed of LDHs platelets, forming hierarchical LDHs/Al_2O_3 fiber composites. As compared to bare LDHs particles and Al_2O_3 fibers, the LDHs/Al_2O_3 composites exhibit excellent adsorption properties. The equilibrium adsorption data were well-fitted to the Langmuir model, while the second-order kinetic model provided the better correlation of the kinetic data. This work not only provides a simple approach to fabricate hierarchically porous materials by low cost papers, but also gives an excellent adsorbent for fluoride adsorption in pollution control.

ACKNOWLEDGEMENTS

The authors would like to thank Jenna Shorten for her helpful comments and suggestions and the financial support from NSFC (No. 51077013) is also acknowledged.

REFERENCES

1. A. Abbas, A. Brimer, J. M. Slocik, L. Tian, R. R. Naik and S. Singamaneni, *Anal. Chem.*, **85**, 3977 (2013).
2. S. Chakravarty, S. Pimple, H. T. Chaturvedi, S. Singh and K. K. Gupta, *J. Hazard. Mater.*, **159**, 396 (2008).
3. S. Pitsari, E. Tsoufakis and M. Loizidou, *Chem. Eng. J.*, **223**, 18 (2013).
4. S. K. Srivastava, A. K. Singh and A. Sharma, *Environ. Technol.*, **15**, 353 (1994).
5. S. Mandal and S. Mayadevi, *Appl. Clay Sci.*, **40**, 54 (2008).
6. A. Bhatnagar, E. Kumar and M. Sillanpää, *Chem. Eng. J.*, **171**, 811 (2011).
7. Q. Guo and Q. Guo, *Environ. Technol.*, **34**, 1053 (2012).
8. M. Mohapatra, S. Anand, B. K. Mishra, D. E. Giles and P. Singh, *J. Environ. Manage.*, **91**, 67 (2009).
9. T. Zhang, Q. Li, H. Xiao, Z. Mei, H. Lu and Y. Zhou, *Appl. Clay Sci.*, **72**, 117 (2013).
10. X. Xu, Q. Li, H. Cui, J. Pang, H. An, W. Wang, et al., *Environ. Technol.*, **33**, 1409 (2011).
11. M. Pontié, H. Dach, J. Leparc, M. Hafsi and A. Lhassani, *Desalination*, **221**, 174 (2008).
12. N. Kabay, Ö. Arar, S. Samatya, Ü. Yüksel and M. Yüksel, *J. Hazard. Mater.*, **153**, 107 (2008).
13. T. Zhang, Q. Li, H. Xiao, H. Lu and Y. Zhou, *Ind. Eng. Chem. Res.*, **51**, 11490 (2012).
14. S. Jagtap, M. K. Yenkie, N. Labhsetwar and S. Rayalu, *Chem. Rev.*, **112**, 2454 (2012).
15. T. Zhang, Q. Li, Y. Liu, Y. Duan and W. Zhang, *Chem. Eng. J.*, **168**, 665 (2011).
16. H. Liu, S. Deng, Z. Li, G. Yu and J. Huang, *J. Hazard. Mater.*, **179**, 424 (2010).
17. T. Zhang, Y. Zhou, M. He, Y. Zhu, X. Bu and Y. Wang, *Chem. Eng. J.*, **219**, 278 (2013).
18. L. Li, R. Ma, Y. Ebina, N. Iyi and T. Sasaki, *Chem. Mater.*, **17**, 4386 (2005).
19. M. Karthikeyan, K. K. Satheesh Kumar and K. P. Elango, *J. Fluorine Chem.*, **130**, 894 (2009).
20. S. R. Shirsath, A. P. Patil, R. Patil, J. B. Naik, P. R. Gogate and S. H. Sonawane, *Ultrason. Sonochem.*, **20**, 914 (2013).
21. Y. Çengeloglu, E. Kir and M. Ersöz, *Sep. Purif. Technol.*, **28**, 81 (2002).
22. M. S. Onyango, Y. Kojima, O. Aoyi, E. C. Bernardo and H. Matsuda, *J. Colloid Interface Sci.*, **279**, 341 (2004).
23. B. Kemer, D. Ozdes, A. Gundogdu, V. N. Bulut, C. Duran and M. Soylak, *J. Hazard. Mater.*, **168**, 888 (2009).
24. L. Lv, J. He, M. Wei, D. G. Evans and X. Duan, *J. Hazard. Mater.*, **133**, 119 (2006).
25. W. S. W. Ngah and S. Fatinathan, *J. Environ. Manage.*, **91**, 958 (2009).
26. B. Pangeni, H. Paudyal, K. Inoue, H. Kawakita, K. Ohto, H. Harada, et al., *Environ. Technol.*, **33**, 845 (2011).
27. E. Malkoc and Y. Nuhoglu, *Chem. Eng. Process.*, **46**, 1020 (2007).
28. M. Chabani, A. Amrane and A. Bensmaili, *Chem. Eng. J.*, **125**, 111 (2006).
29. Y. S. Ho, *Water Res.*, **40**, 119 (2006).
30. Y. S. Ho and G. McKay, *Water Res.*, **34**, 735 (2000).
31. P. H. Chen, C.-F. Hsu, D. D.-W. Tsai, Y.-M. Lu and W.-J. Huang, *Environ. Technol.*, **35**, 1935 (2014).